INTEGRATION OF BOTTOM ELECTRODE IN Y-CUT LITHIUM NIOBATE THIN FILMS FOR HIGH ELECTROMECHANICAL COUPLING AND HIGH CAPACITANCE PER UNIT AREA MEMS RESONATORS

Abhay Kochhar, Luca Colombo, Gabriel Vidal-Álvarez, and Gianluca Piazza
Carnegie Mellon University, Pittsburgh, USA

ABSTRACT

This paper reports the integration of a bottom electrode in thin films of Y-cut lithium niobate (LN) on silicon to demonstrate high performance lamb-wave (S0 mode) and thickness-shear-mode (TSM) resonators. The LN resonator is sandwiched between top and bottom electrodes and attained high coupling (k_t^2) > 6% when excited in S0 mode and > 30% when excited in TSM. The reported devices possess capacitance per unit area of 0.4 fF/um^2, which is 30 times that of X-cut LN and 5 times that of AlN resonators. This demonstration enables MEMS designers to fully harness the high coupling of thin LN films, which can have a transformative impact on reconfigurable and ultra-low-power communication systems.

INTRODUCTION

Recent work on MEMS resonators has focused on attaining high k_t^2 so as to enable tunability, reconfiguration and programmability of RF functionalities over a wide bandwidth [1-3]. Focus has been placed on thin films of LN which intrinsically possesses a high k_t^2 when excited in specific modes of vibration. Previously reported thin-film-based LN resonators [3-5] have shown high coupling, but did not attain a large capacitance per unit area required to match to 50 Ω, a basic need for many RF applications including reconfigurable [6] and ultra-low-power communication systems [7-8]. A fundamental bottleneck of these resonator implementations has been the lack of a bottom electrode and hence the need for a very large footprint to match to the RF system impedance. This has either resulted in the need to array small resonators (with associated frequency matching challenges) or low yields because of residual stresses in the suspended membrane.

In this work, we demonstrate a high capacitance per unit area (i.e. a 30x reduction in footprint with respect to prior LN resonator implementations) by incorporating a bottom electrode in thin films of Y-cut LN. In the same process, we demonstrate S0-mode and TSM resonators. The former is of great interest because it enables multiple frequencies on the same chip [9], the latter because, like quartz crystal microbalances, it can be used extensively in oscillators, temperature, pressure and bio sensors [10], as well as fixed filters for communication links.

RESONATOR DESIGN AND FABRICATION PROCESS

The vibrating resonators of this work are made of interdigital electrodes (also called as fingers in this paper) on
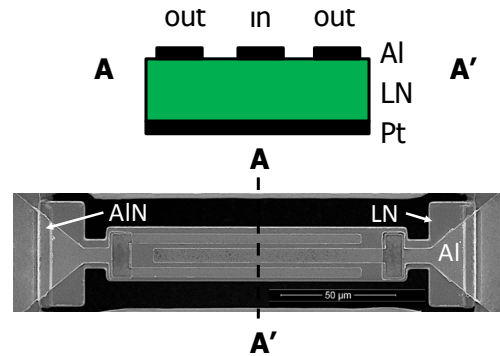

Figure 1: Cross-section and SEM image of the Y-cut lithium niobate resonator developed in this work. The top electrode is patterned to form interdigital fingers. A bottom electrode was introduced for the first time with LN films. In this paper, the bottom electrode is used in a floating configuration.

top of the Y-cut LN piezoelectric film (Fig. 1). A continuous layer of Pt is used for the bottom electrode. Utilizing a bottom electrode helps in increasing the resonator capacitance and with proper via configuration makes the realization of true two-port networks possible. The S0 mode is excited when the applied electric field (either lateral or vertical) produces lateral expansion and compression in the resonator body. The vertically applied field utilizes the finger to bottom electrode's capacitance as compared to fringe (finger to finger) capacitance when the electric field is applied laterally (without bottom electrode). This approach dramatically increases the device's total capacitance per unit area, especially for frequencies below 1 GHz. The thickness-shear mode (TSM) is generated when the electric potential is applied across the film thickness and results in a shear stress developing across the two faces orthogonal to the film thickness. In this work the bottom electrode was left floating, which ensures that high coupling can be attained without the need for vias.

This new class of LN resonators was made possible by: 1) the ion-slicing of LN wafer and direct-bonding to Pt-coated silicon wafers; 2) the development of a fabrication process compatible with an un-patterned bottom electrode; 3) the selection of the LN cut to enable resonator designs vibrating in either the S0 or TSM by means of interdigitated top electrodes. The device synthesis was made possible by separately patterning the LN film and the Pt bottom electrode as well as using a thin AlN film to suspend the LN resonator. The use of the AlN film was necessary to support the device, but was also selected because of the AlN acoustic properties which should enable greater acoustic impedance mismatch at

the anchors. By using Y-cut LN, the devices were designed to vibrate at 200, 400 and 600 MHz in the S0 mode (set by the pitch of the electrodes) and around 1.3 GHz in the TSM (set by the film thickness). The electrode coverage for these designed resonators were 50 %. The resonators mode of vibration and expected admittance response were analyzed using 3D COMSOL FEA (see Figure 9). The resonator's equivalent electrical parameters were extracted by fitting the responses to a Modified Butterworth-Van Dyke (MBVD) model [11].

The fabrication process flow that was used to build the devices presented in this paper is shown in Figure 2. The substrate was produced according to the techniques described in [12] and procured from Partow Inc. The etch sidewall of LN was kept as straight as possible to mitigate damping [13]. PECVD deposited SiO_2 film was used as a mask for patterning the LN film. A thin Cr film was sputtered on SiO_2, patterned and dry etched so that it forms a hard mask for the definition of the SiO_2 layer. Photolithography was performed using a NIKON stepper with AZ4110 as a photoresist for the Cr pattern. This pattern defines the release and device areas for the LN resonator. After defining the patterns, the photoresist was removed in 1165 microposit remover
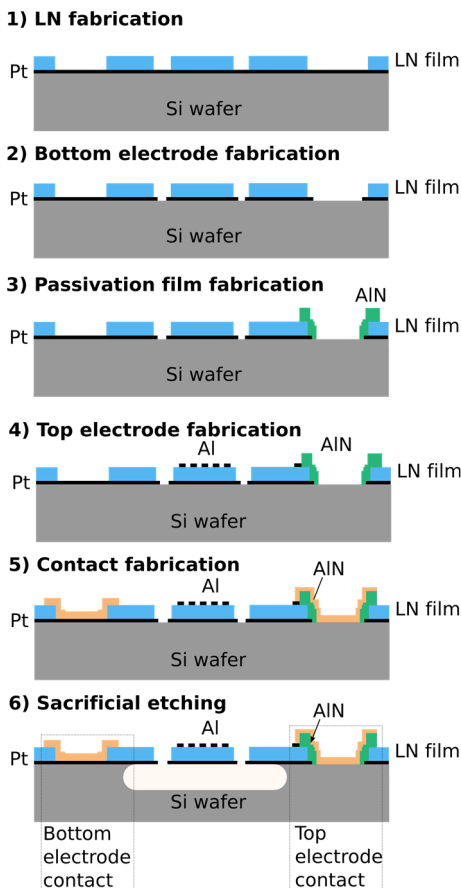

Figure 2: *Fabrication process flow of the resonator utilizing bottom electrode. This flow shows the ability to form vias to the bottom electrode. Vias did not work for the devices presented in this paper, yielding a device configuration with a floating bottom electrode.*

solution heated at 50 °C. For SiO_2 etching, F-based parallel plate RIE was used. For Cr, LN and Pt etch, a combination of Cl_2 and BCl_3 gas based ICP RIE was utilized. The final etch of the last few 300 nm of LN, right before reaching the Pt electrode layer, was done in an ion-milling machine equipped with a secondary ion mass spectrometry (SIMS), which is capable of detecting when Pt is reached. After LN etching, the SiO_2 mask was removed using F-based parallel-plate RIE, which has a minimal attack on the lithium niobate film. Pt was patterned using AZ4110 photoresist in the same stepper and dry etched. Photoresist was removed in acetone for 1 hour with ultrasonic agitation. Later, 1 μm of aluminum nitride was sputtered using Tegal's AC reactive sputtering tool operating at 7 kW. The patterning of the film was done by using a 4 μm thick AZ4400 photoresist. For better etch control and selectivity, the photoresist was hard baked at 150 °C for 30 min in an oven. CD-26 having 2.4 % of tetramethyl-ammounium-hydroxide (TMAH) was used as a wet etchant for the AlN film. The solution was heated up to 55 °C to achieve an approximate etch rate of the AlN film of about 200 nm/min. For uniformity purposes, a magnetic stirrer was utilized. Aluminum nitride was used as a support and anchor for the lithium niobate plate. Top electrode and contact fabrication (both aluminum) were patterned using a lift-off process. For lift-off, acetone with ultrasonic agitation was utilized. To lift-off fine patterns in the case of the top electrode, heated (at 80 °C) 1165 microposit remover was utilized. IPA rinse following Semitool's spin rinser/dryer was used for cleaning the wafer. Finally, the silicon underneath the device area was etched using XeF_2 vapor phase etching.

EXPERIMENTAL RESULTS

The SEM image of one of the fabricated devices is shown in Figure 1. The sidewall of the LN film after etching is shown in Figure 3, confirming that an angle better than 80º could be attained. Multiple devices with varying total capacitance and frequency of operation were tested. The device measurements were performed with an Agilent's VNA and the collected data were analyzed using MATLAB. The devices ended up using the bottom electrode in a floating configuration and were tested by connecting the two ports of the VNA to the two terminals of the device referred to as Port 1 and Port 2 in Figure 4. The measured S-parameters were converted into Y parameters and the Y21 are used to describe the resonators' performance in this paper.

S0 mode resonators

The devices vibrating in the S0 mode exhibited k_t^2 between 3 and 6% with Qs from 100 to 1,000. The microscope image of a device operating at 600 MHz is shown in Fig. 4. The same layout was used for a device operating at 200 MHz, but with a different pitch size and overall plate width. The characteristic response (magnitude of the device admittance) for resonators operating around 600 MHz and
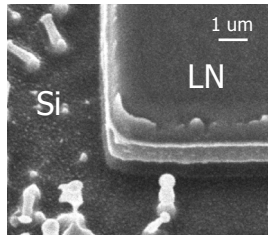
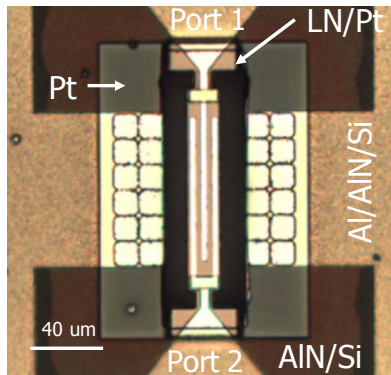Figure 3: Sidewall of the etched LN using Cl_2-based ICP-RIE.

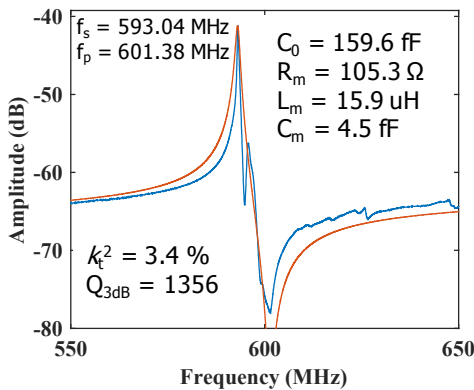Figure 4: Microscope image of a Y-cut resonator after fabrication

Figure 5: Frequency response of the three finger device designed to operate at 600 MHz (4.5 μm pitch).

200 MHz is shown in Figures 5 and 6, respectively. The equivalent dielectric constant and velocity (of the film stack) are evaluated as 45 and 5530 m/sec, respectively. The capacitance per unit area corresponds to 0.4 fF/μm^2 as compared to the 0.08 fF/μm^2 that one could achieve in similar AlN devices.

TSM resonators

Theoretically, the TSM resonator in Y-cut LN could possess an electromechanical factor as high as $K_{24} = 72\%$ (notations are with respect to Z-cut LN material properties), hence having the capability to demonstrate a k_t^2 of 51%. Experimental measurement of TSM resonators exhibited k_t^2 ranging between 20 and 33% with Qs between 50 and 200 at around 1.3 GHz. Figures 7 and 8 show the characteristic responses of some of the tested devices, which exhibited k_t^2
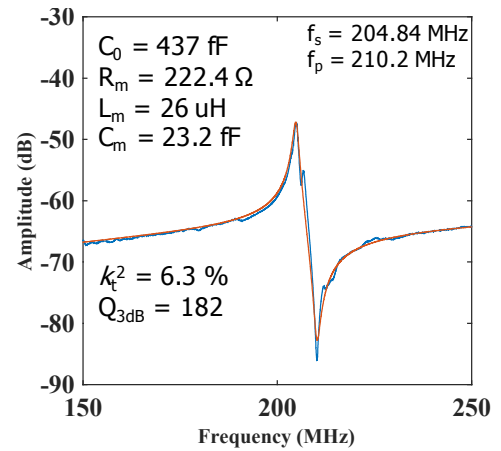

Figure 6: Frequency response of a three finger Y-cut resonator designed to work at 200 MHz (13.5 μm pitch).

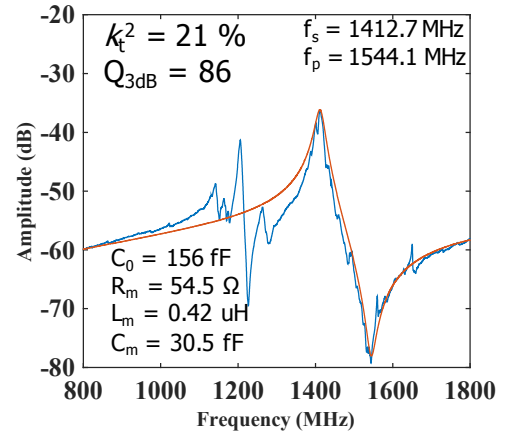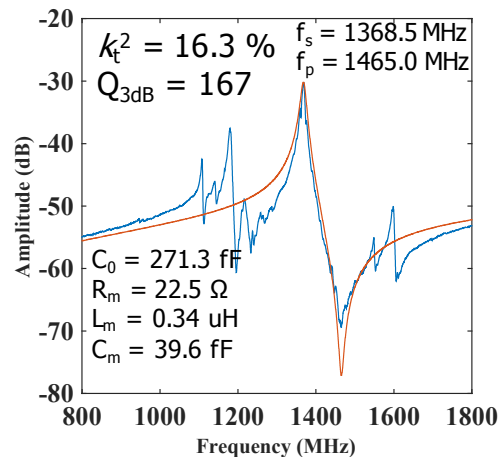Figure 7: TSM mode in a three finger resonator with an electrode pitch of 4.5 μm.

Figure 8: TSM mode in a four finger device with different electrode pitch (6.5 μm)

of 16% and 21%, respectively. The length of the fingers is 84 μm and 56 μm, respectively.

Finally, the experimental data were compared to simulations performed using 2D COMSOL finite element analysis (FEA). A fixed damping factor was used in the simulations. Fig. 9 shows the mode of vibration and expected admittance response for two specific devices having the same geometry and capable of vibrating in both the S0 and TSM

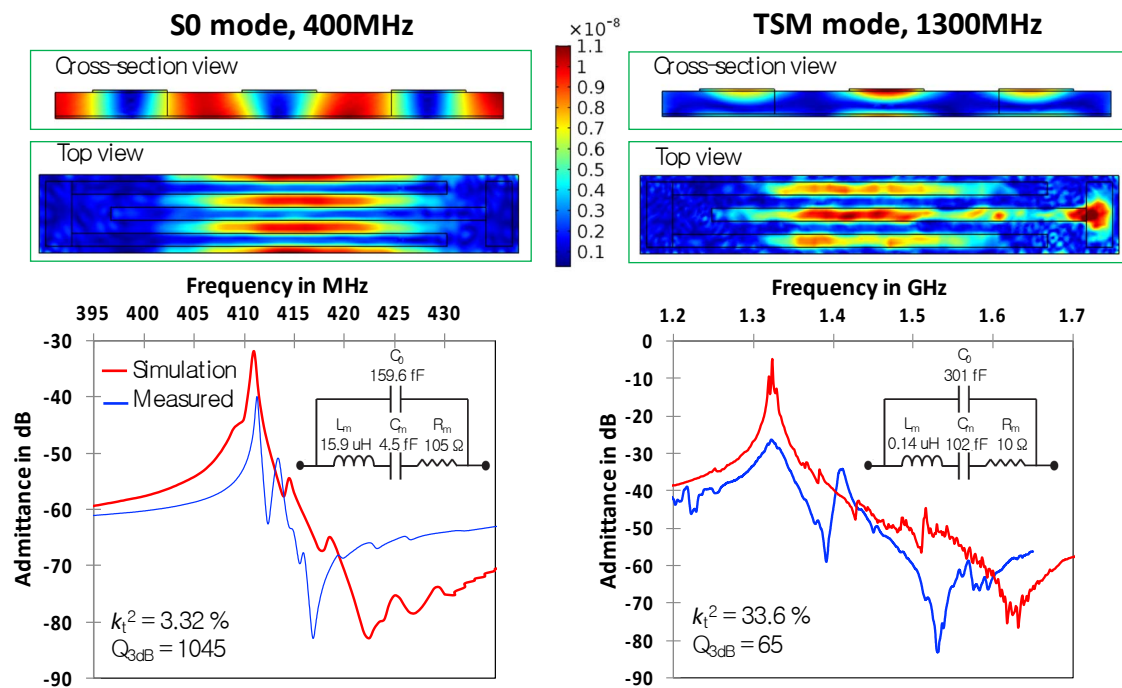**S0 mode, 400MHz**

TSM mode, 1300MHz

Figure 9: Cross-section, top-view of the total displacement and simulated vs measured admittance response for (a) S0 mode resonator working at 400MHz, and (b) TSM resonator working at around 1.3GHz. The electrode pitch is 6.5 µm. The equivalent parameters, shown in the inset of the admittance responses are extracted by fitting to the measured device.

modes. This comparison shows that the experimental data are far from attaining the ultimate performance that these devices are capable of. Proper routing and patterning of the bottom electrode will permit to devise resonators capable of exhibiting much higher k_t^2. The sources of damping in these resonators are still unknown and would have to be subject of future investigations.

CONCLUSION

This paper presents the integration of bottom electrode in transferred films of lithium niobate, hence enabling the making of a new class of high coupling resonators capable of attaining a high capacitance per unit area. This implementation shows promising results in term of electromechanical coupling coefficient and Q. Improving the Q of these resonators should be the subject of future investigations. Similarly, the ability to define vias to the bottom electrode will enable the implementation of true 2-port devices, which will improve out-of-resonance signal rejection. Our demonstrated Y-cut LN platform enables the implementation of devices with much smaller area than any reported piezoelectric MEMS resonator with high performance and allows practical use of LN devices in 50 Ω RF systems.

ACKNOWLEDGEMENTS

REFERENCES

[1] T. Yasue et al., 16th International Solid-State Sensors, Actuators and Microsystems Conference, pp. 1488-1491, 2011.
[2] S. Gong, et. al., 17th International Conference on Solid-State Sensors, Actuators and Microsystems, pp. 2465-2468, 2013.
[3] M. Kadota and S. Tanaka, Japanese Journal of Applied Physics, Vol. 55, No. 7S1, pp. 07KD041 – 6, 2016.
[4] T. Kimura, et. al., Japanese Journal of Applied Physics, Vol. 53, No. 7S, pp. 07HD031 – 4, 2013.
[5] R. Wang, et. al., IEEE Micro Electro Mechanical Systems (MEMS), pp. 165-168, 2013.
[6] M. Rais-Zadeh, et. al., Proceedings of the IEEE, vol. 103, no. 3, pp. 438-451, March 2015.
[7] J. M. Rabaey et. al., IEEE Intl. Solid-State Circuits Conf., Vol. 45, pp. 200-201, 2002.
[8] J. Blanckenstein, J. Klaue and H. Karl, in IEEE Circuits and Systems Magazine, vol. 15, no. 3, pp. 6-17, 2015.
[9] S. Gong and G. Piazza, Journal of Microelectromechanical Systems, vol. 23, no. 5, pp. 1188-1197, Oct. 2014.
[10] E. P. EerNisse and R. B. Wiggins, IEEE Sensors Journal, vol. 1, no. 1, pp. 79-87, June 2001.
[11] J. D. Larson, P. D. Bradley, S. Wartenberg and R. C. Ruby, IEEE Ultrasonics Symposium, 2000, pp. 863-868.
[12] P. Rabiei, et. al., Opt. Express 21, 25573-25581 (2013).
[13] S. Gong and G. Piazza, IEEE Transactions on Electron Devices, vol. 60, no. 11, pp. 3888-3894, Nov. 2013.

CONTACT

*Abhay Kochhar; abhay.kochhar@ieee.org